Infinite Science Publishing

Proceedings Article

Two-Step Reconstruction with Spatially Adaptive Regularization for Increasing the Dynamic Range in MPI

Marija Boberg [a,b,*] · Tobias Knopp [a,b]

[a] Section for Biomedical Imaging, University Medical Center Hamburg-Eppendorf, Hamburg, Germany
[b] Institute for Biomedical Imaging, Hamburg University of Technology, Hamburg, Germany
*Corresponding author, email: m.boberg@uke.de

Abstract

Magnetic particle imaging is capable of determining very small concentrations of particles if only a single concentration is present in the field-of-view. Meanwhile the determination of particles with widely differing concentrations is still challenging. In a recent work, we introduced a two-step reconstruction method that tackles this problem by isolating the signal of the lower concentrated tracer for a separate reconstruction. In this work, we adapt the two-step reconstruction method in order to apply a joint reconstruction to the entire signal of all particle concentrations. This is achieved by spatially adaptive Tikhonov regularization.

I. Introduction

Magnetic particle imaging (MPI) is used to determine the spatial distribution of superparamagnetic iron-oxide nanoparticles. In a scenario where only a single particle concentration is present in the field-of-view, MPI is capable of determining a large idealized dynamic range with a minimum of about $5\,\text{ng}_{\text{Fe}}$ [1]. In typical in-vivo measurements there often is higher tracer concentration in the vascular system, while the concentration is much lower in some organs like the kidneys. The effective dynamic range of different concentrations in the same field-of-view that MPI is capable of imaging is considerably smaller than the idealized dynamic range. In [2], a simple two-step reconstruction algorithm was introduced that is able to enlarge the effective dynamic range. In order to achieve this, the higher and lower concentrations were reconstructed separately. In this work, we propose an alternative second step with a spatially adaptive regularization for a joint reconstruction of the different concentrations. This avoids artifacts stemming from the

difficulty to accurately separate the higher from the lower concentrations.

II. Methods and Materials

The discrete MPI signal equation is given by

$$\hat{\boldsymbol{u}} = \boldsymbol{S}\boldsymbol{c}$$

where $\boldsymbol{c} \in \mathbb{R}_+^N$ is a vector with N voxels describing the particle distribution, $\hat{\boldsymbol{u}} \in \mathbb{C}^K$ denotes the Fourier transformed measured voltage signal with K frequency components, and $\boldsymbol{S} \in \mathbb{C}^{K \times N}$ is the system matrix. With a regularized reconstruction

$$\boldsymbol{R}_{\mathscr{P}}(\boldsymbol{S}, \hat{\boldsymbol{u}}) =$$
$$\text{solve}_\iota\left(\underset{\boldsymbol{c} \in \mathbb{R}_+^N}{\text{argmin}} \left\| \tilde{\boldsymbol{P}}_\Theta(\boldsymbol{S})\boldsymbol{c} - \boldsymbol{P}_\Theta(\hat{\boldsymbol{u}}) \right\|_2^2 + \|\Lambda\boldsymbol{c}\|_2^2 \right), \quad (1)$$

the particle distribution is then obtained from the measured signal. Here, three different regularization methods are combined for an optimal noise reduction. First,

the Tikhonov regularization with the penalization term (last summand) with the parameter $\Lambda \in \mathbb{R}^{N \times N}$ prevents large oscillations of c. The projections $P_\Theta : \mathbb{C}^K \to \mathbb{C}^{K_\Theta}$ and $\tilde{P}_\Theta : \mathbb{C}^{K \times N} \to \mathbb{C}^{K_\Theta \times N}$ describe a frequency selection choosing only frequency components with a signal-to-noise ratio larger than the parameter $\Theta \in \mathbb{R}_+$. This reduces noise in the solution similarly to the Tikhonov regularization. Finally, solve_ι is an iterative solver restricted to $\iota \in \mathbb{N}$ iterations so that c is not fitted too much to the noise. All regularization methods come with a decrease in spatial resolution, which requires problem specific parameters to trade off between low spatial resolution and noisy reconstruction results. All regularization parameter are combined in the variable $\mathscr{P} = (\Lambda, \Theta, \iota)$. For the sake of convenience, we set $\Lambda = \lambda I_N$ as a diagonal matrix if the regularization parameter is given as a scalar $\lambda \in \mathbb{R}$.

II.I. Two-Step Reconstruction

Since varying particle concentrations require different regularization parameters we propose the following two-step reconstruction algorithm that combines two reconstructions with different regularization parameters. An initial reconstruction identifies areas with higher concentrated tracer. This is used to build a problem specific Tikhonov matrix for the second reconstruction. The algorithm gets as input the acquired data $\hat{u}$, the system matrix S, a threshold $\Gamma \in [0, 1]$, and two parameter sets $\mathscr{P}_{\text{high}} = (\lambda_{\text{high}}, \Theta_{\text{high}}, \iota_{\text{high}})$ and $\mathscr{P}_{\text{low}} = (\lambda_{\text{low}}, \Theta_{\text{low}}, \iota_{\text{low}})$.

1. *First reconstruction* of the measurement data using parameter $\mathscr{P}_{\text{high}}$ suitable for higher concentrations:

$$c_{\text{pre}} = R_{\mathscr{P}_{\text{high}}}(S, \hat{u}).$$

2. *Thresholding* of the reconstruction result to separate higher and lower concentrated parts of the image:

$$(c_{\text{thresh}})_n = \begin{cases} (c_{\text{pre}})_n, & \text{if } |(c_{\text{pre}})_n| \geq \Gamma \|c_{\text{pre}}\|_\infty \\ 0, & \text{else.} \end{cases}$$

3. *Adapting the Tikhonov matrix*

$$(\Lambda_{\text{low}}^{\text{pre}})_{n,n} = \begin{cases} \lambda_{\text{low}} & \text{if } (c_{\text{thresh}})_n = 0 \\ \lambda_{\text{high}} & \text{else.} \end{cases}$$

yielding $\tilde{\mathscr{P}}_{\text{low}} = (\Lambda_{\text{low}}^{\text{pre}}, \Theta_{\text{low}}, \iota_{\text{low}})$.

4. *Second reconstruction* using the parameter $\tilde{\mathscr{P}}_{\text{low}}$:

$$c_{\text{final}} = R_{\tilde{\mathscr{P}}_{\text{low}}}(S, \hat{u}).$$

III. Experiments

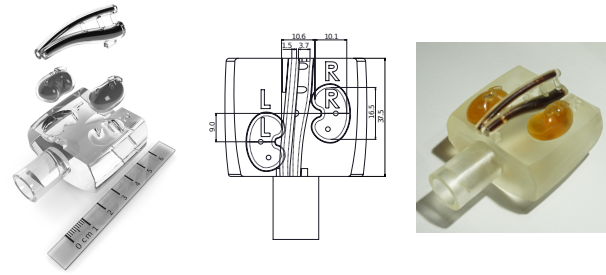The proposed method is tested with a realistic rat phantom consisting of two kidneys and a part of the vessels

Figure 1: Anatomic rat phantom with replaceable kidneys and vessels.

shown in Fig. 1. The vessels are filled with $306\,\mu\text{L}$ and each kidney with $781\,\mu\text{L}$ diluted perimag as tracer material. The concentration of the kidneys is chosen as $\kappa_i = 2^{-(4+i)}\kappa_\nu$, $i = 1, 2, 3$, where $\kappa_\nu = 100\,\text{mmol}_{\text{Fe}}\,\text{L}^{-1}$ denotes the concentration of the vessels. Further information on the phantom can be found in [2].

Measurements were performed with a pre-clinical MPI system 25/20FF (Bruker Corporation, Ettlingen, Germany), which applied a 3D Lissajous trajectory using a gradient strength of $(-0.75, -0.75, 1.5)\,\text{T m}^{-1}$ and $12\,\text{mT}$ drive-field amplitude in all three directions. The system matrix was acquired at $21 \times 21 \times 24$ positions covering a volume of $42 \times 42 \times 24\,\text{mm}^3$ with a delta sample of size $2 \times 2 \times 1\,\text{mm}^3$.

Image reconstruction of (1) is done with the iterative Kaczmarz solver using the Julia package `MPIReco.jl` [3]. Analogously to [2], the parameter set $\mathscr{P}_{\text{high}} = (0.001, 2, 3)$ is used for the first reconstruction of the higher concentrated vessels. The threshold is set to $\Gamma = 0.2$. For this reconstruction method, we additionally set $(c_{\text{thresh}})_n = (c_{\text{pre}})_n$ in an area with two pixel width around the region masked with $\Gamma \|c_{\text{pre}}\|_\infty$. The second parameter set $\mathscr{P}_{\text{low}}^i = (\lambda_i, 10, 20)$ with $\lambda_i \in \{0.5, 1, 2\}$ is chosen individually for each concentration of the kidneys. For all reconstructions, only frequencies above $80\,\text{kHz}$ are used. Note that in our implementation, the regularization parameter is scaled with $\text{trace}(\tilde{P}_\Theta(S)^H \tilde{P}_\Theta(S))N^{-1}$. For comparison, we apply the method from [2] with the parameters used there. The only exception is a general threshold $\Gamma_2 = 0.08$ for all concentrations, which we use here to avoid a noise dominated result of the first reconstruction, which would also dominate the combined reconstruction result.

IV. Results and Discussion

Fig. 2 shows the results of a regular reconstruction with (1) using different parameter sets and the two-step reconstruction from our proposed method compared to [2].

The first row shows good reconstruction results of the kidneys using the parameter set $\mathscr{P}_{\text{low}}^i$. Thus, the regular
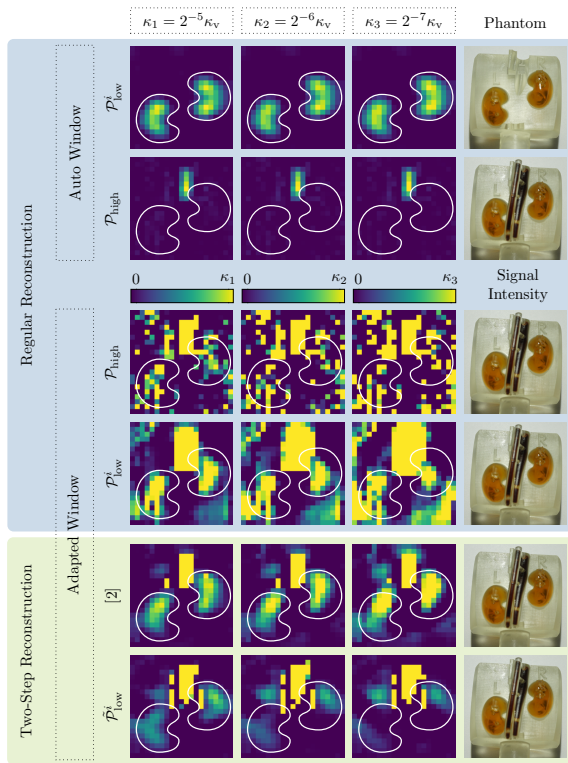
Figure 2: Reconstruction results using the regular reconstruction with different parameter sets and the two-step reconstructions proposed in [2] and here.

Kaczmarz reconstruction is able to reconstruct the low concentrated kidneys. These reconstructions are used to mark the position and shape of the kidneys in each image of the figure. If the vessels are placed between the kidneys, reconstruction with the parameter set $\mathscr{P}_{high}$ is not able to visualize the kidneys neither with an auto window (second row) nor with an adapted window (third row), where the color range is normalized to the range $[0, \kappa_i]$. In the reconstructed images using the parameter set $\mathscr{P}_{low}^i$ shown in the fourth row, some signal at the position of the kidneys is visible. But it does not have the shape of the kidneys and also some artifacts in other regions of the image appear. The lower the concentration of the kidneys, the higher are the artifacts. Therefore, the kidneys are not separable from the artifacts for κ_2 and κ_3. Both two-step reconstructions in the last two rows are improving the results and show less artifacts. The kidneys are clearly detectable for κ_1, while from κ_2 on, the shape of the signal vanishes into a more artifact-like shape stemming from the vessels. However, the artifacts are less prominent using the joint reconstruction (last row). Then, also the shape of the left kidney is more accurate for κ_1. The lines next to the vessel stem from the additional area around the vessels where we also used λ_{high} in the Tikhonov matrix as the regularization parameter.

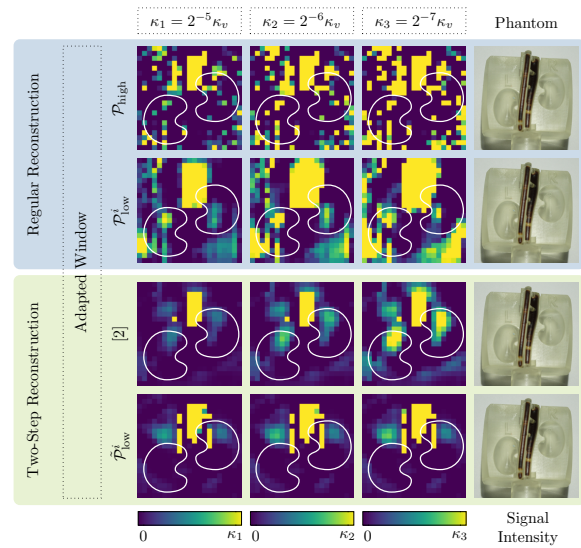For comparison, all reconstruction methods are also

Figure 3: Reconstruction results of the vessels without kidneys using the same methods and parameters as in Fig. 2.

applied to the phantom without kidneys, which is shown in Fig. 3. The reconstruction results emphasize which artifacts are stemming from the vessels and can be mistaken as kidneys in Fig. 2. Only the joint method is able to suppress artifacts in the region of the kidneys for all three reconstructions.

V. Conclusion

In summary, both two-step reconstruction approaches are able to improve the reconstruction results and enlarge the effective dynamic range. The main difference of the two-step reconstruction using a spatially adaptive regularization to the method proposed in [2] is the joint reconstruction of the entire signal in the last step. In [2], a threshold was used to separate the lower concentrated parts and reconstruct them separately in the second reconstruction step. Both two-step reconstruction methods reduce artifacts distracting from lower concentrated tracer. The method from [2] yields a more accurate mean concentration in the kidneys compared to the joint reconstruction with adaptive regularization. The latter yields a more accurate shape of the kidneys. It also provides better artifact reduction so that artifacts are not mistaken to be particles. Overall, both methods offer a different but simple approach for enlarging the effective dynamic range in MPI.

Author's statement

References

[1] M. Graeser, T. Knopp, P. Szwargulski, T. Friedrich, A. von Gladiss, M. Kaul, K. M. Krishnan, H. Ittrich, G. Adam, and T. M. Buzug. Towards picogram detection of superparamagnetic iron-oxide particles using a gradiometric receive coil. *Scientific Reports*, 7:6872, 2017, doi:10.1038/s41598-017-06992-5.

[2] M. Boberg, N. Gdaniec, P. Szwargulski, F. Werner, M. Möddel, and T. Knopp. Simultaneous imaging of widely differing particle concentrations in MPI: Problem statement and algorithmic proposal for improvement, 66(9):095004, 2021, doi:10.1088/1361-6560/abf202.

[3] T. Knopp, P. Szwargulski, F. Griese, M. Grosser, M. Boberg, and M. Möddel. MPIReco.jl: Julia package for image reconstruction in MPI. *International Journal on Magnetic Particle Imaging*, 5(1), 2019, doi:10.18416/ijmpi.2019.1907001.